

c.1



RESEARCH MEMORANDUM

EXPERIMENTAL INVESTIGATION TO DETERMINE THE LOADS

A HORIZONTAL TAIL OF A MODEL CAUSED

BY A BLAST-INDUCED GUST

By Harold B. Pierce and Raymond J. Spahl

Langley Aeronautical Laboratory
Langley Field, Va.

LIBRARY COPY

APR 11 1957

LANGLEY AERONAUTICAL LABORATORY
LIBRARY, NACA
LANGLEY FIELD, VIRGINIA

CLASSIFIED DOCUMENT

This material contains information affecting the National Defense of the United States within the meaning of the espionage laws, Title 18, U.S.C., Secs. 793 and 794, the transmission or revelation of which in any manner to an unauthorized person is prohibited by law.

NATIONAL ADVISORY COMMITTEE FOR AERONAUTICS

WASHINGTON

March 29, 1957

CLASSIFICATION CHANGED

UNCLASSIFIED

copy of TPA # 33 Date 10-29-68 ERG



UNCLASSIFIED



NATIONAL ADVISORY COMMITTEE FOR AERONAUTICS

UNCLASSIFIED

RESEARCH MEMORANDUM

EXPERIMENTAL INVESTIGATION TO DETERMINE THE LOADS
ON A HORIZONTAL TAIL OF A MODEL CAUSED
BY A BLAST-INDUCED GUST

By Harold B. Pierce and Raymond J. Spahl

SUMMARY

An experimental investigation has been undertaken to examine the type of loading imposed on the horizontal tail of an airplane model due to an intense blast-induced gust which strikes from a direction normal to the flight path. A comparison of the time histories of the incremental load coefficient for the wing and tail surfaces indicated that, for an angle of attack well above the stall condition, a traveling load peak was present on both the wing and tail surfaces and that the load peaks were equal in magnitude. These load peaks are attributed to a vortex formation produced by the diffraction of the shock wave around the leading edge of the airfoil. The similarity of the loading on the wing and tail continued until the tail was affected by the downwash from the wing. When this condition occurred the loading on the tail decreased abruptly.

INTRODUCTION

A blast-induced gust from a direction normal to the airplane wing will strike both the wing and the tail simultaneously and will produce equal angle-of-attack changes on each surface. When the angle of attack due to the gust is initially well beyond the stall, the flow and lift relationships on the wing are very complex and appear to include separation phenomena as well as vortices produced by the diffraction of the shock wave around the wing. (See ref. 1.) It might be expected that the horizontal tail would experience the same complex loading and also unusual downwash effects from the wing. In order to obtain some insight into the type of loading imposed on a horizontal tail under the very high angle-of-attack condition, tests were conducted with a low-speed model subjected to blast-induced gusts caused by actual explosions.



UNCLASSIFIED

This paper presents the results of three flights in which resultant pressures were measured at five points along one chord of the horizontal tail and, for comparative purposes, at five points along one wing chord. The results are given in the form of time histories of load coefficient at each station rather than as load distributions since five points along a chord were not considered to be sufficient to define the distribution under complex-flow conditions.

APPARATUS AND TESTS

A line drawing of the model used in the tests is shown as figure 1. The position of the tail-chord line along which the differential pressures were measured is indicated in figure 1. Also shown is the position of the chord line on the wing where differential pressure measurements were made for comparison with the data obtained along the tail chord. The pressure measurements were made with NACA miniature electrical pressure gages of the type described in reference 2. Five of these cells were imbedded in the flat portion of the horizontal tail at the 10-, 20-, 30-, 40-, and 60-percent-chord station. A section drawing showing the cells and the profile of the airfoil shape is shown in figure 2(a). It may be noted that the tail airfoil section was simply a flat plate 1/4 inch thick with rounded leading edge and tapered trailing edge. The five pressure cells along the wing chord were imbedded in a split aluminum rib in the manner shown in figure 2(b). The orifice locations on the wing were at the 5-, 19-, 37-, 68-, and 84-percent-chord stations. Other characteristics of the model are as follows:

Weight, W, lb	31.75
Wing area, S, sq ft	3.72
Wing loading, W/S, lb/sq ft	8.53
Span, b, ft	5.95
Mean geometric chord, ft	0.625
Aspect ratio, b^2/S	9.51
Wing airfoil section	NACA 0009-64
Center-of-gravity position, percent mean chord	24.3
Pitching moment of inertia, slug-ft ²	0.624

With the exception of the horizontal tail and minor changes in weight and weight distribution, the present model is the same as that used in the investigation of reference 1.

The tests were performed at Wallops Island, Va., in the blast area north of the Langley Pilotless Aircraft Research Station. The test technique used is illustrated schematically in figure 3. The model, powered by a self-contained rocket, was trimmed for zero lift and

launched at a high angle from the horizontal. The timing was set so that, at rocket burnout, the model was moving tangent to the shock front from the explosion. By this technique, the blast-induced gust struck from a direction normal to the flight path at a time when the forward speed of the model could be considered to be constant. The differential pressures measured by the gages in the tail and wing were transmitted to a ground receiving station by a wire telemeter. The forward speed, position, and attitude of the model were determined from pictures taken by two 70-millimeter motion-picture cameras, one located in the y,z plane of the model and the other in the x,z plane of the model. All records used common timing and synchronization sources. The operations, such as turning on cameras, recorders, and firing of the model, were controlled by a programmer having steps of 1 second. A delay timer capable of being set to 0.02 second, started by the initial movement of the model, was used to explode the charge at the proper time.

In order to examine the type of loading imposed on the horizontal tail by a blast-induced gust causing a very large angle-of-attack change, the test conditions were the same as those used in reference 1. These conditions specified that the blast-induced gust initially increase the angle-of-attack about four times above the steady-flow stall angle of the model. An angle-of-attack change of this magnitude was chosen to insure that not only would the maximum angle of attack in the gust be in the steady-flow stall region for the model but also that it would be nearly twice the stall angle for the full-scale airfoil section. In order to fulfill these conditions, the forward velocity of the model at blast encounter was approximately 114 feet per second and the initial gust velocity was about 75 feet per second.

The blast-induced gusts were produced by the explosion of 150-pound hemispherical charges of the plastic explosive, Composition C-3. The charges were mounted 5.3 feet above the ground and about 200 feet from the point of tangency of the flight path with the resultant shock front. Preliminary tests showed that, with the charge located in this manner, the model would be in the Mach stem region, that is, the region where the shock wave reflected from the ground has overtaken and combined with the initial airborne shock wave (ref. 3). The strength of this combined shock front closely approximated that of a 300-pound charge exploded in free air.

Since it was not possible to measure the gust velocities directly at the model, the gust velocities were calculated from pressure measurements made with two pole-mounted blast gages in the test area. The blast gages consisted of an NACA miniature electrical pressure gage at the center of a 1/8-inch-thick aluminum disk 18 inches in diameter. One blast gage was mounted 10 feet above the ground on a pole 200 feet from the explosive charge and 20 feet from the launching position of the model. The second gage was mounted 50 feet above the ground, 226.5 feet

from the charge, and 170 feet from the launching site. They were oriented so that the faces of the gages were rotated to an angle of 5° from the side-on position toward the blast. Time histories of the blast-wave overpressure (increase of pressure above atmospheric pressure) were measured by the gages and the results are presented in figures 4(a) and 4(b). It may be noted that only one gage was operative for flight 1, whereas both gages produced records in flights 2 and 3. The records shown were faired for the first 4 milliseconds since the instantaneous pressure jump at the shock front caused high-frequency oscillation of the gage diaphragms or gage ringing during this period.

In order to determine the true peak pressure produced by the blast at the gages, an empirical curve often used in blast work for such cases was fitted to the overpressure time histories of figure 4. The equation of the empirical curve used is presented in appendix II of reference 4 as:

$$P = P_S \left(1 - \frac{T}{\tau} \right) e^{-cT/\tau}$$

where

- P excess pressure (overpressure)
- P_S peak excess pressure
- T time ($T = 0$ at the time of arrival of the shock wave)
- τ positive duration (that is, time that pressure in blast wave is in excess of atmospheric pressure)
- c constant for a particular wave

A value of $1/2$ for the constant c was suggested by the Ballistic Research Laboratories at Aberdeen Proving Ground, Maryland, to provide the degree of curvature that would best fit the pressure-time history of the shock waves obtained in this test. An example of the fit obtained is shown in figure 5.

In order to determine the gust velocities at the model, it was necessary to transfer the pressure histories for the gage locations to the position of the model. For this purpose, data on the variation of peak overpressure with distance from a blast, such as given in reference 5, were utilized. The gust histories at the model were then calculated by the Rankine-Hugoniot shock-wave equations (ref. 6) and are shown in figure 6. Figure 7 presents the angle-of-attack variation for each flight as determined from the change in the relative wind vector produced by the gust striking the model.

A summary of the conditions for each flight is presented in table I. The table shows that there was some variation between the flights in maximum gust velocity, forward velocity of the model, and the angle between the flight path and the gust. These variations, however, are not considered to affect the results significantly.

PRECISION

The measured quantities are estimated to be accurate within the following limits for any test or run:

Forward velocity, ft/sec	±3
Overpressure, percent	±5
Differential pressure on model, percent	±2
Angle of attack, deg	±2

The pressure records from the model for the first 2 milliseconds after blast arrival are not considered reliable. Although the measuring system is usable to frequencies of 1,000 cycles per second, the instantaneous pressure rise in the shock wave produced frequencies beyond the range of the system.

When the time history of angle of attack caused by the gust was determined, no corrections were made for wing flexibility and model motion. As shown in reference 1, these effects were small, particularly in the early portions of the time history where the gust angle is large.

RESULTS

Time histories of the incremental load coefficient $\frac{\Delta p_R}{q}$ were determined for each active station on the tail and wing for each flight. The evaluation of the dynamic pressure q was based on the variation of the resultant velocity caused by the blast-induced gust and the accompanying change in air density. The incremental resultant pressure Δp_R for each active station on the tail and wing was obtained from the telemetered pressure records for each flight. Figure 8(a) to 8(e) present the time histories of the incremental load coefficient for each station on the tail. Figures 9(a) to 9(e) present the time histories of the incremental load coefficient for each station on the wing. The first 2 milliseconds of the histories were deleted because of the erratic behavior of the measuring system during this period. Because of an instrument malfunction, the time history of the load coefficient at the 5-percent station on the wing for the third flight was not presented in figure 9(a).

It may be noted from figures 8 and 9 that the results of flights 1 and 2 appear to be consistent; the results of flights 3, in general, show a lower peak pressure and a less rapid rate of attenuation as compared with flights 1 and 2. The time histories of load coefficient for the rearmost measuring stations on the tail and wing (figs. 8(e) and 9(e)) are erratic. This condition is considered to be a result of separation of flow over the rear portion of the airfoil, the separation effects being more pronounced on the flat-plate tail than on the airfoil-shaped wing.

DISCUSSION

The time histories of the load coefficient given in figures 8 and 9 show a load peak on both the tail and wing. This load peak is similar to that found in the pressure distributions given in reference 1 and is again attributed to a traveling vortex formed initially by the diffraction of the blast wave around the leading edge of the surface. It may also be observed that, in the later portion of the time histories, the direction of the loading on the tail is opposite to that on the wing.

In order to obtain a better understanding of the loading on the tail, average time histories of the three flights were determined for two of the chord stations on the tail and were compared with the average histories for two equivalent stations on the wing. Figure 10(a) presents the comparison of the average histories for the 20-percent-chord station on the tail with the 19-percent station on the wing, and figure 10(b) compares the histories of the 40-percent station on the tail and the 37-percent station on the wing. It may be observed in figure 10 that the magnitude of the load peaks on the tail is very nearly equal to the magnitude of the peaks on the wing and that a similarity exists between the time histories for the wing and tail until approximately 13 milliseconds had elapsed. The loading on the tail then drops abruptly while the loading on the wing appears to experience a more gradual decrease. The abrupt decrease in loading on the tail is apparently caused by the downwash from the wing since the time of 13 milliseconds corresponds closely to the lag in the time required for the wing downwash to reach the tail. Although no attempt was made to evaluate the overall effect of the downwash for the tail, it may be noted from figure 10 that the extent of the abrupt drop in loading on the tail appeared to be of the order of 70 to 80 percent of the first maximum load at each station. Thus, it would appear that the effect of downwash considerably complicates the tail loading.

The load peak caused by the traveling vortex, which was found on both the wing and the tail, obviously has a significant effect on the loads and also produces drastic variations in the pitching moments on

these surfaces. It may be observed in figures 10(a) and 10(b) that the load peak reaches given-percent chord stations on the tail sooner than it reaches the equivalent stations on the wing. Inasmuch as many unsteady flow phenomena are functions of aerodynamic time (that is, chord-length travel of the surface), the data of figure 10 were replotted as a function of aerodynamic time and are presented in figures 11(a) and 11(b). In figure 11, it is seen that the load peaks nearly coincide for the two stations along the chords of the wing and tail. As a result, it appears that the movement of the load peak on the wing and tail of an airplane is primarily a function of the chord-length travel of the surfaces although other factors, such as shock strength or leading-edge radius, also probably influence the travel of the vortex. For the condition of this test and that of reference 1, the load peaks appear to move from the leading edge to the trailing edge in approximately three chord-lengths travel of the individual surfaces.

SUMMARY OF RESULTS

The results of an investigation of the type of loading on the horizontal tail due to the effects of an intense blast-induced gust which increased the angles of attack above the stall condition showed that:

1. Traveling load peaks attributed to vortex formations initiated by the diffraction of the blast wave around the leading edge of the airfoils were present on both the tail and the wing.

2. The traveling load peaks on the tail and wing were of equal intensity.

3. The loading histories on the tail and wing were similar until the downwash from the wing reached the tail and caused a reversal of the tail loading.

4. The movement of the load peaks on the tail and wing appeared to be a function of the chord-length travel of the respective surfaces.

Langley Aeronautical Laboratory,
National Advisory Committee for Aeronautics,
Langley Field, Va., January 11, 1957.

REFERENCES

1. Pierce, Harold B., and Reisert, Thomas D.: Initial Experimental Investigation of the Aerodynamic Load on the Wing of a Model Caused by a Blast-Induced Gust That Increases the Angle of Attack Into the Stall Region. NACA RM L55H22b, 1955.
2. Patterson, John L.: A Miniature Electrical Pressure Gage Utilizing a Stretched Flat Diaphragm. NACA TN 2659, 1952.
3. Bryant, E. J., Eberhard, R. A., and Kingery, C. N.: Mach Reflection Over Hard Packed Dirt and Dry Sand. Rep. No. 809, Ballistic Res. Labs., Aberdeen Proving Ground, July 1952.
4. Armendt, B. F., Smith, R., and Wise, R. C.: The Initial Decay of Pressure Behind a Shock Front: Comparison of Experimental and Calculated Results. Memo. Rep. No. 997, Ballistic Res. Labs., Aberdeen Proving Ground, Apr. 1956.
5. Curtis, Wesley: Free Air Blast Measurements on Spherical Pentolite. Memo. Rep. No. 544, Ballistic Res. Labs., Aberdeen Proving Ground, July 1951.
6. Liepmann, Hans Wolfgang, and Puckett, Allen E.: Introduction to Aerodynamics of a Compressible Fluid. John Wiley & Sons, Inc., 1947.

CN 45960

TABLE I.- CONDITIONS AT BLAST-WAVE ARRIVAL

	<u>Flight 1</u>	<u>Flight 2</u>	<u>Flight 3</u>
Maximum overpressure, lb/sq in.	1.45	1.50	1.40
Maximum gust velocity, ft/sec	76.5	79.2	71.5
Angle between flight path and gust, deg . .	88.0	82.3	80.6
Forward velocity of model, ft/sec	124	119	101
Maximum angle-of-attack change, deg	32	31	32
Duration of gust, milliseconds	21	21	24
Distance of model from blast, ft	196	192	189

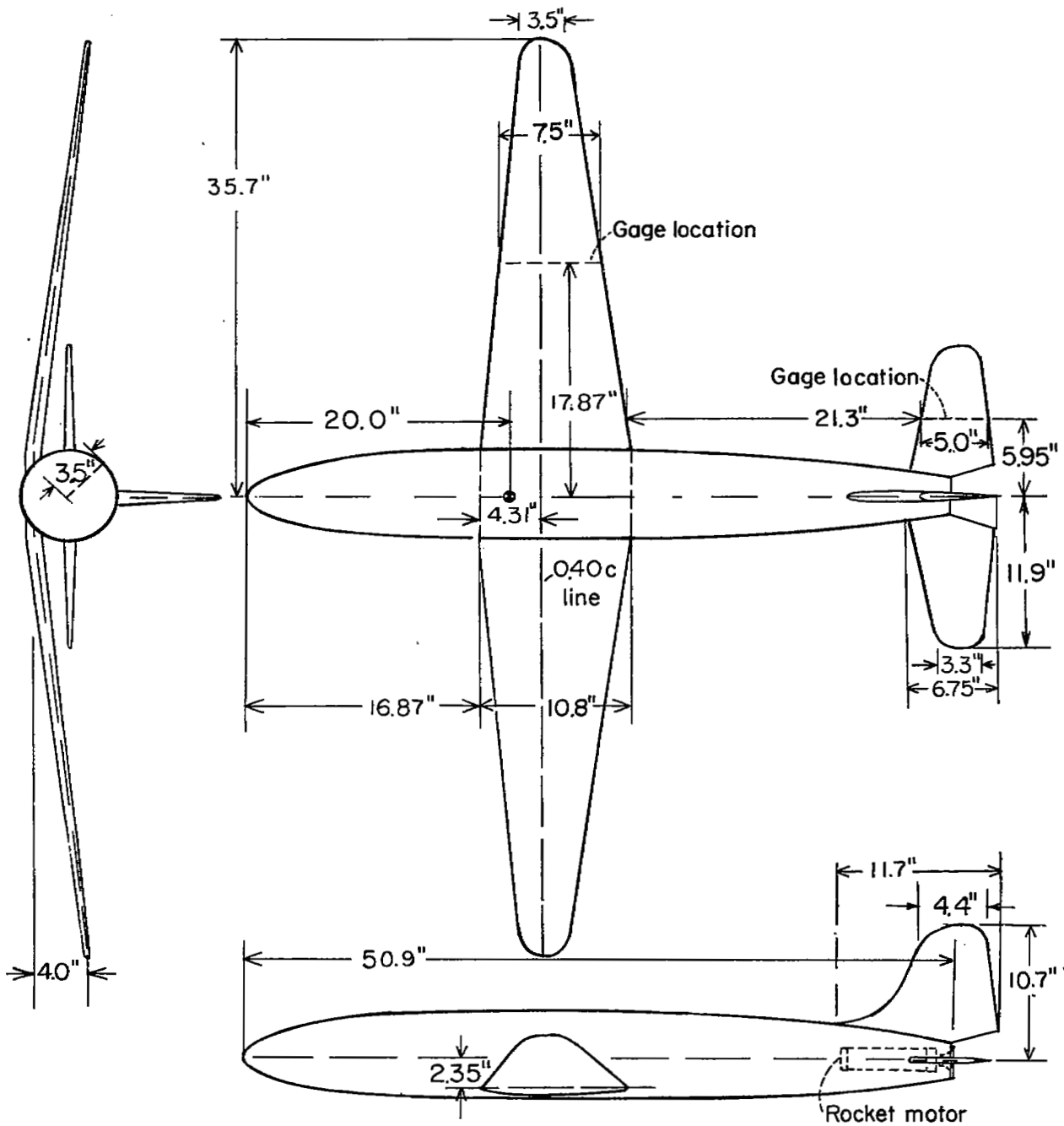
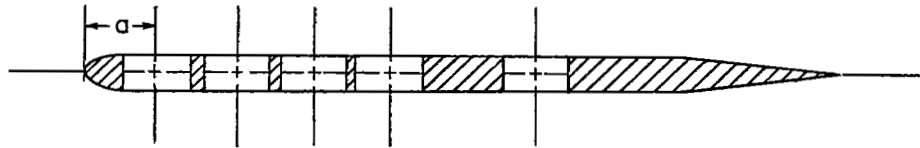
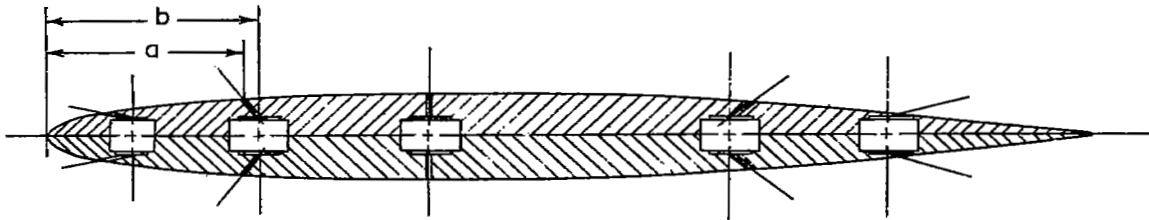


Figure 1.- Three-view drawing of test model.



Orifice location, in. a
.500
1.000
1.500
2.000
3.000

(a) Tail.



Orifice location, in. a	Pressure pick-up location, in. b
.376	.566
1.428	1.543
2.782	2.782
5.112	4.962
6.315	6.115

(b) Wing.

Figure 2.- Pressure-gage installation in wing and tail.

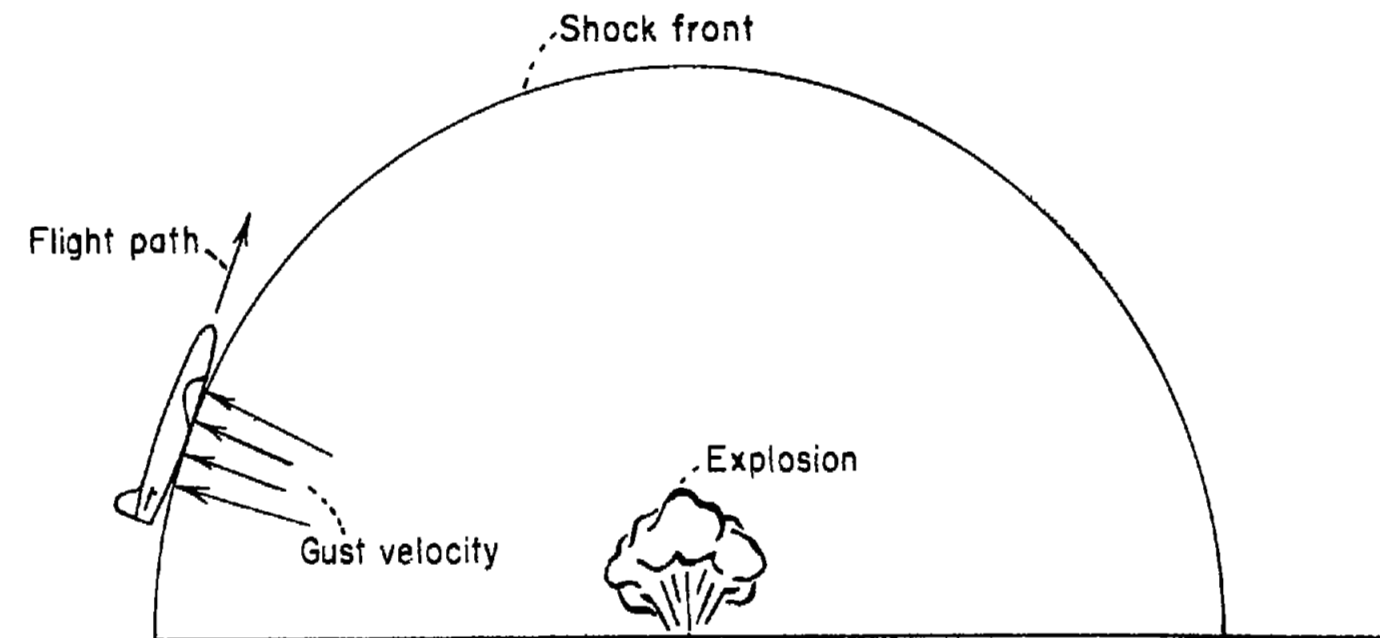


Figure 3.- Conditions at time of shock-front arrival.

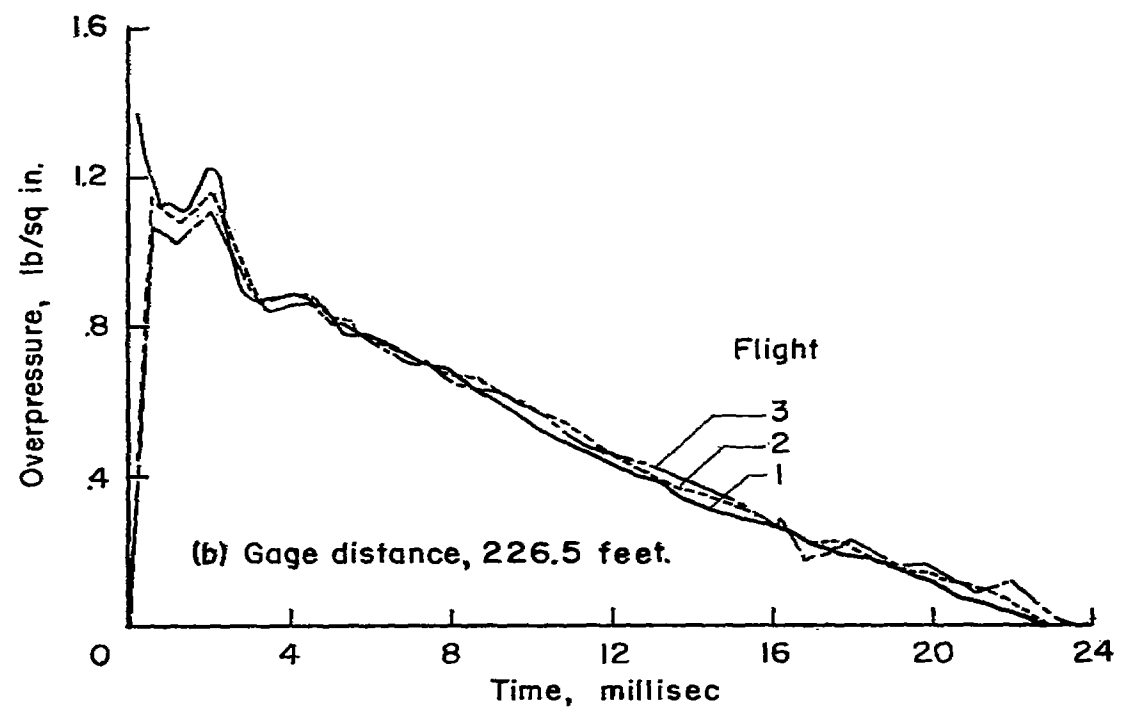
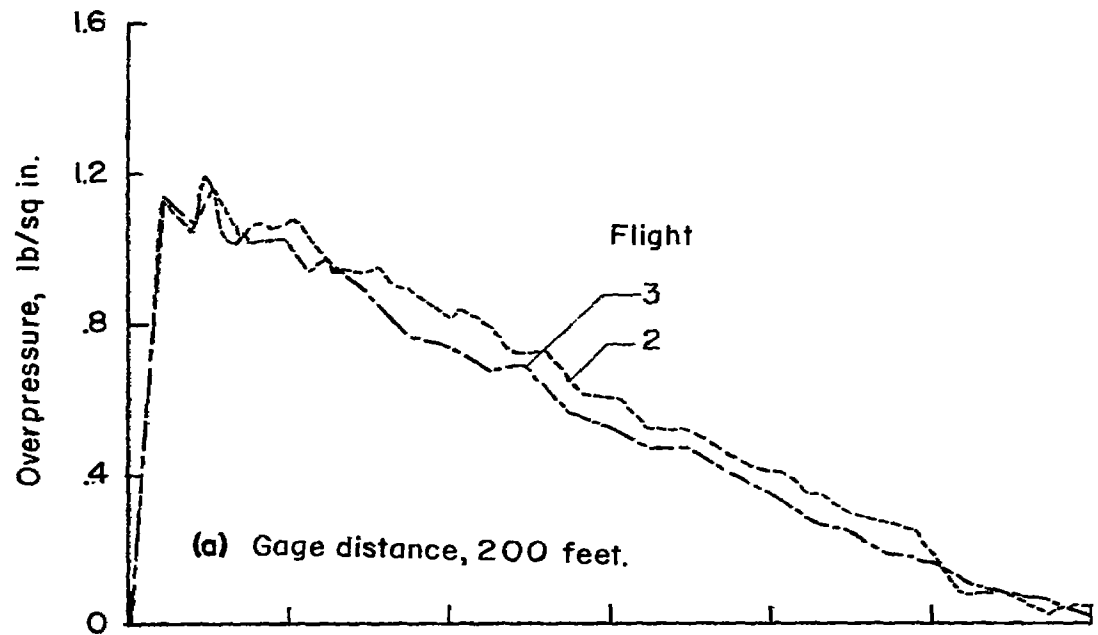


Figure 4.- Time histories of overpressure (at gage stations).

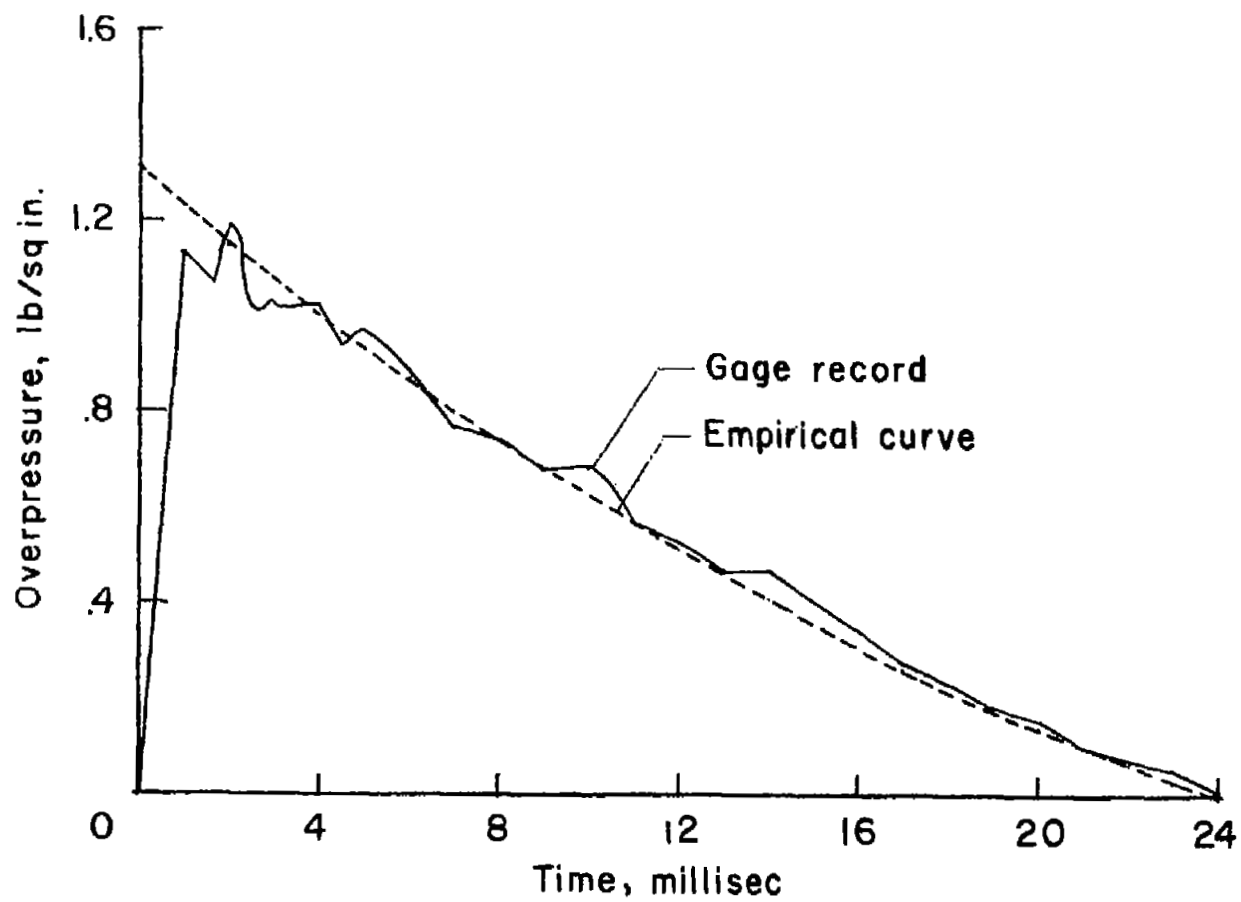


Figure 5.- Fit of empirical curve to gage record.

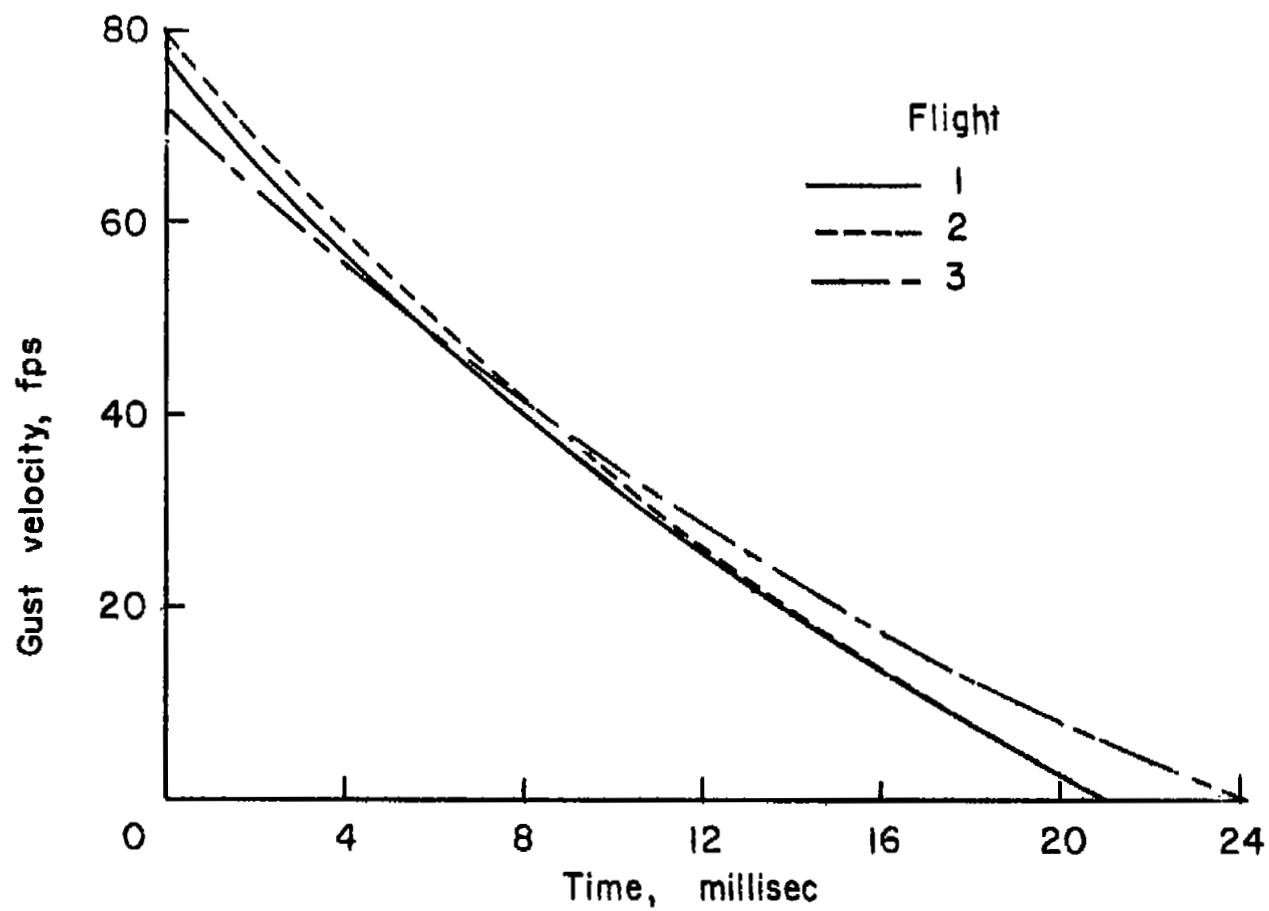


Figure 6.- Time histories of gust velocity (at model).

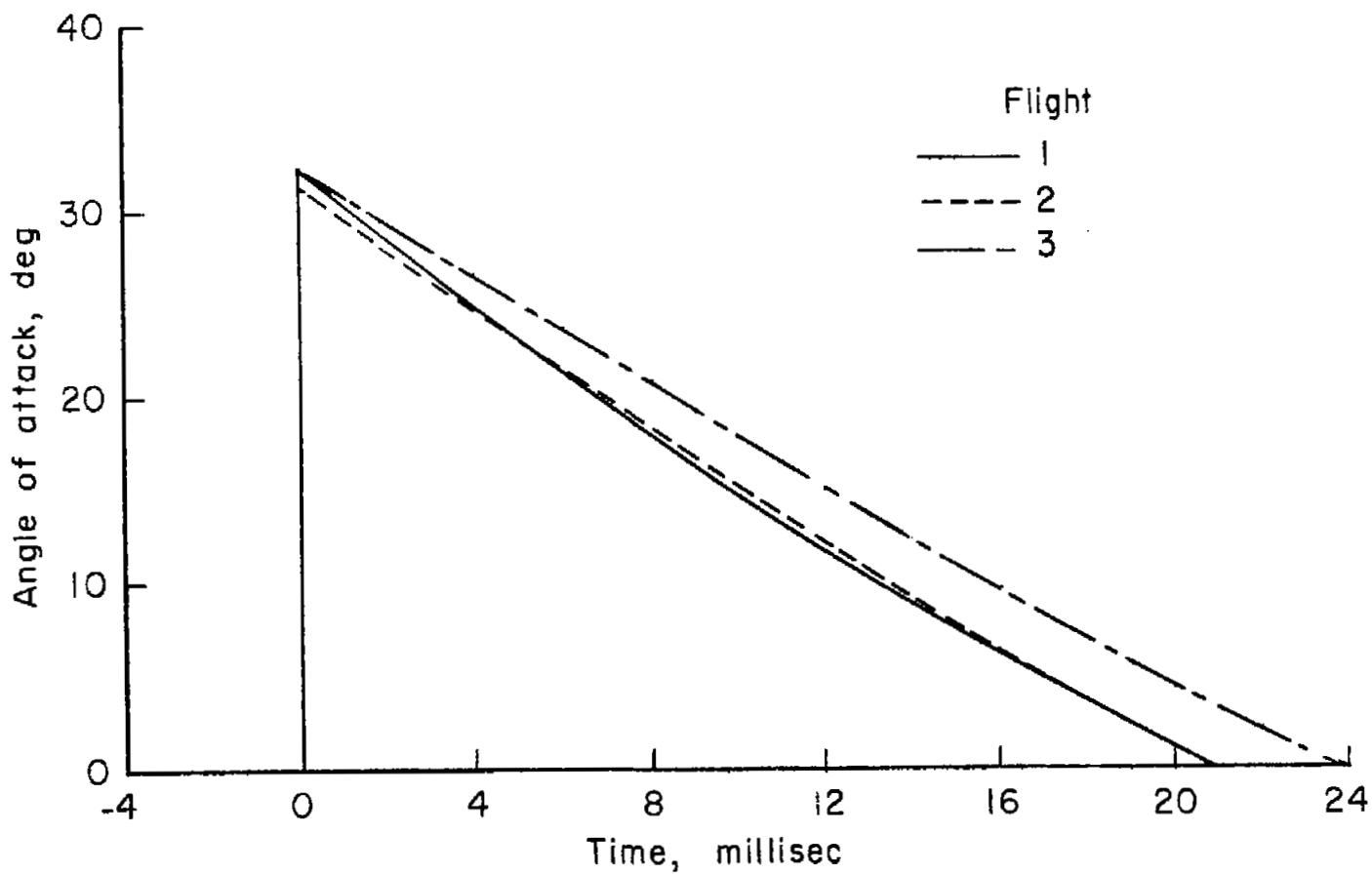


Figure 7.- Time histories of angle of attack (imposed on model).

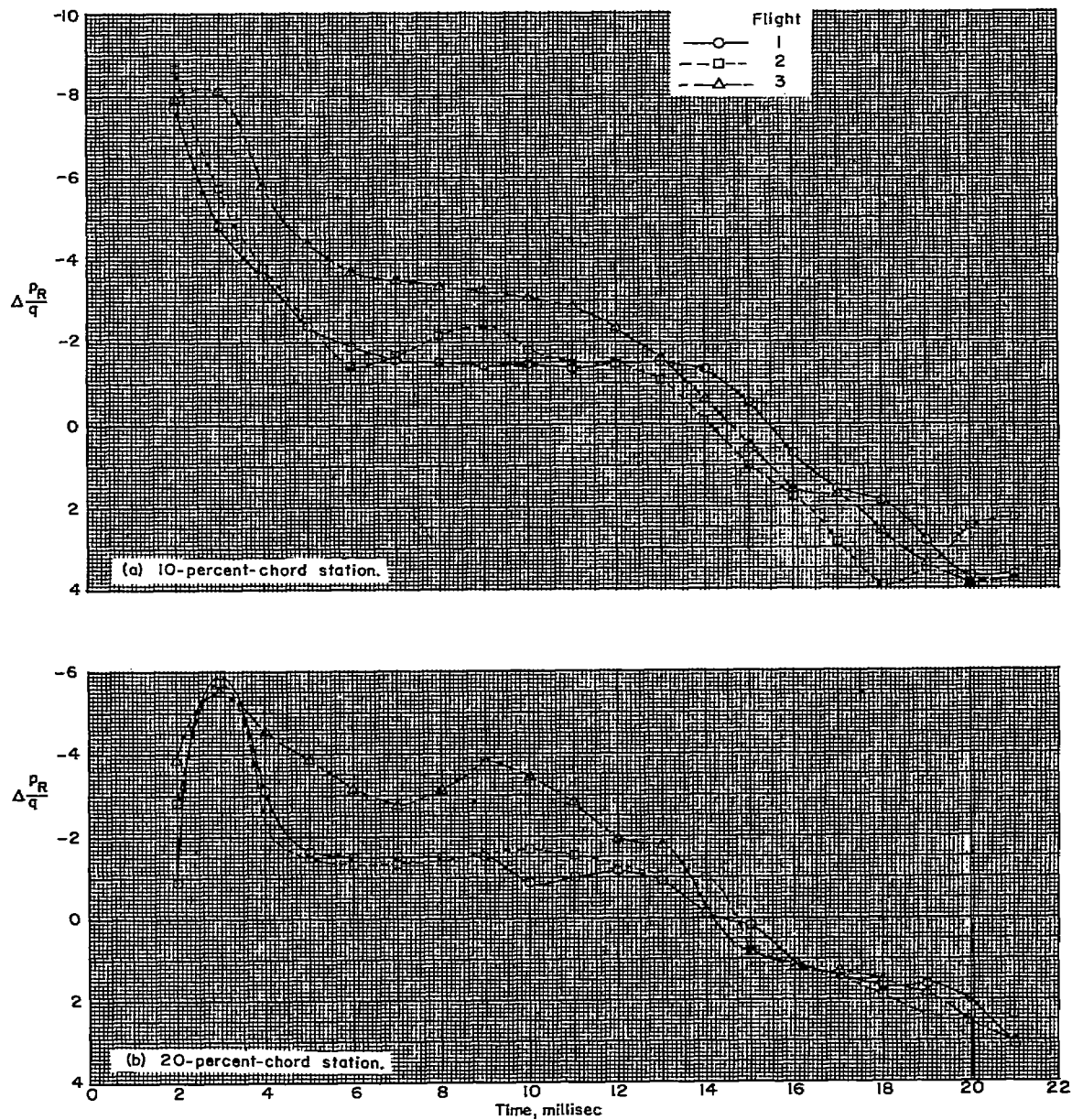


Figure 8.- Time histories of load coefficients on tail.

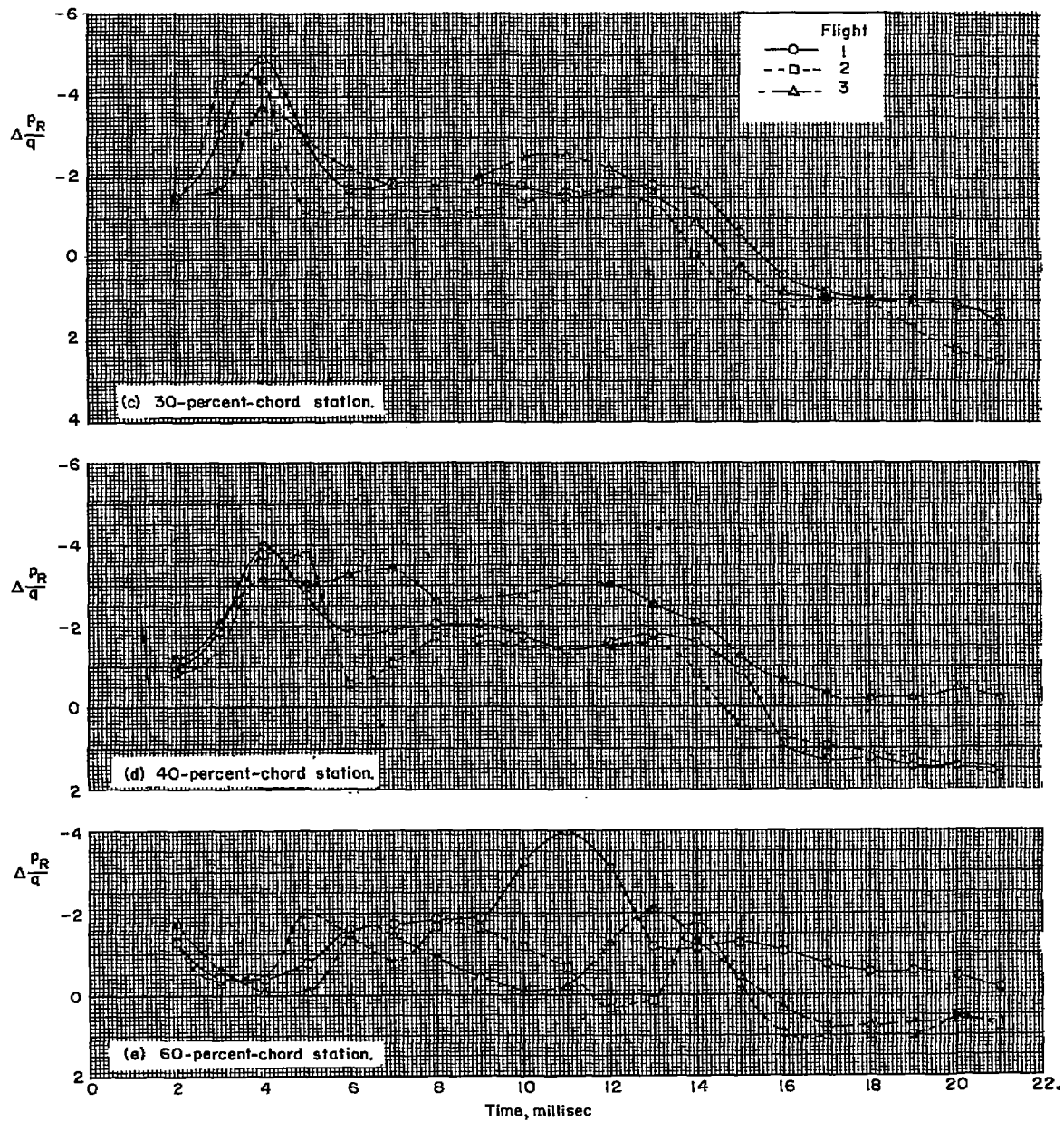


Figure 8.- Concluded.

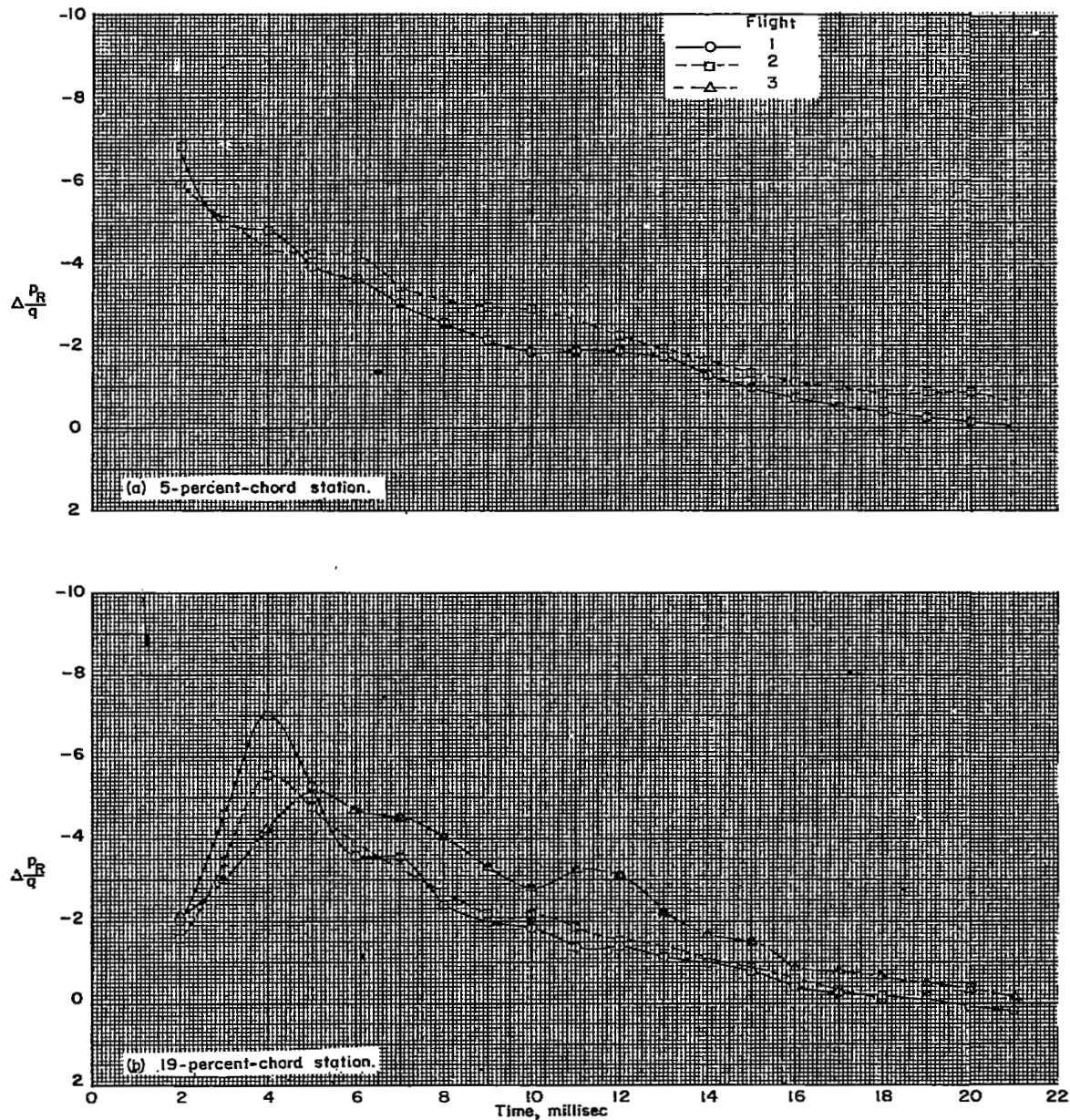


Figure 9.- Time histories of load coefficients on wing.

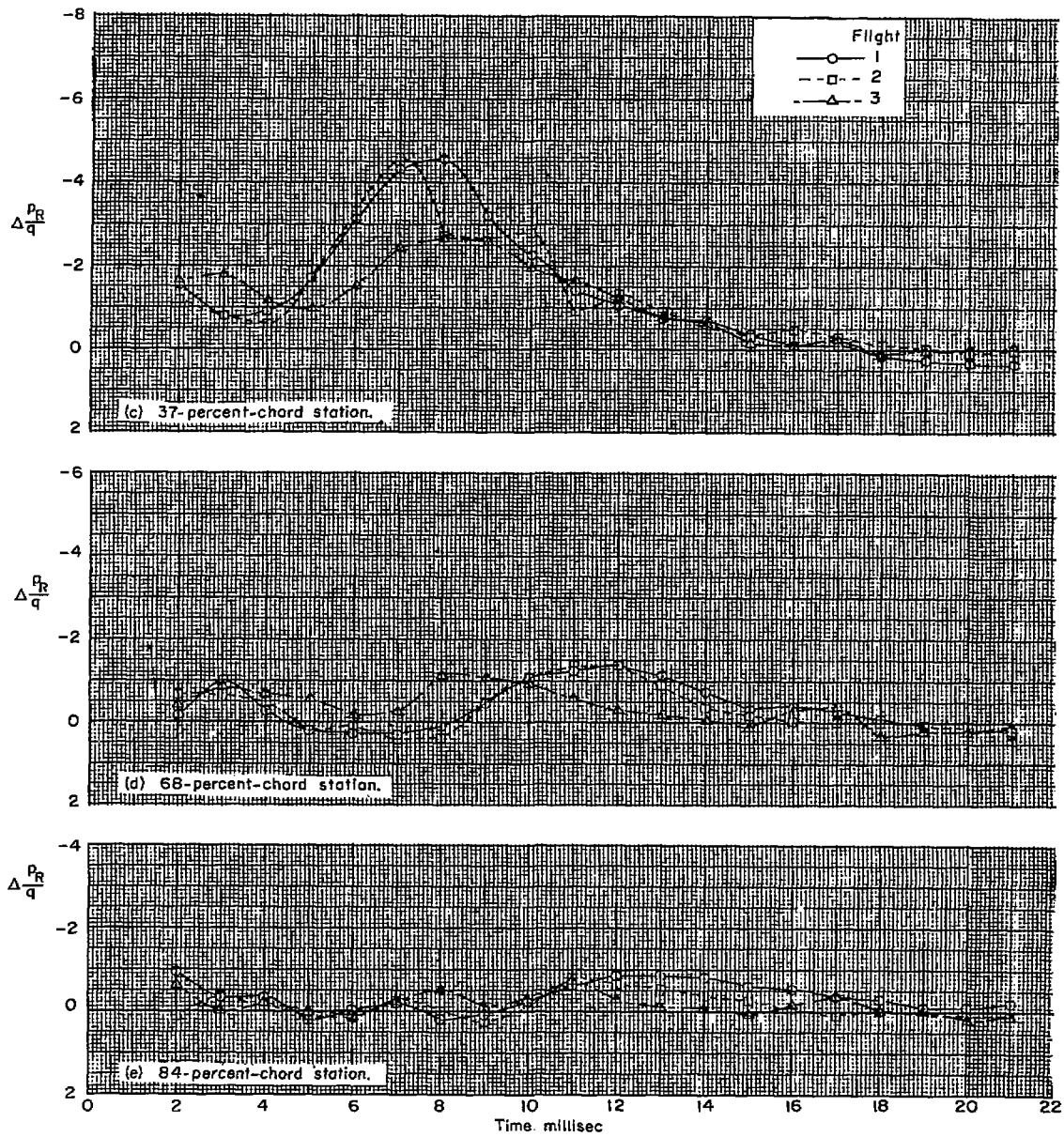
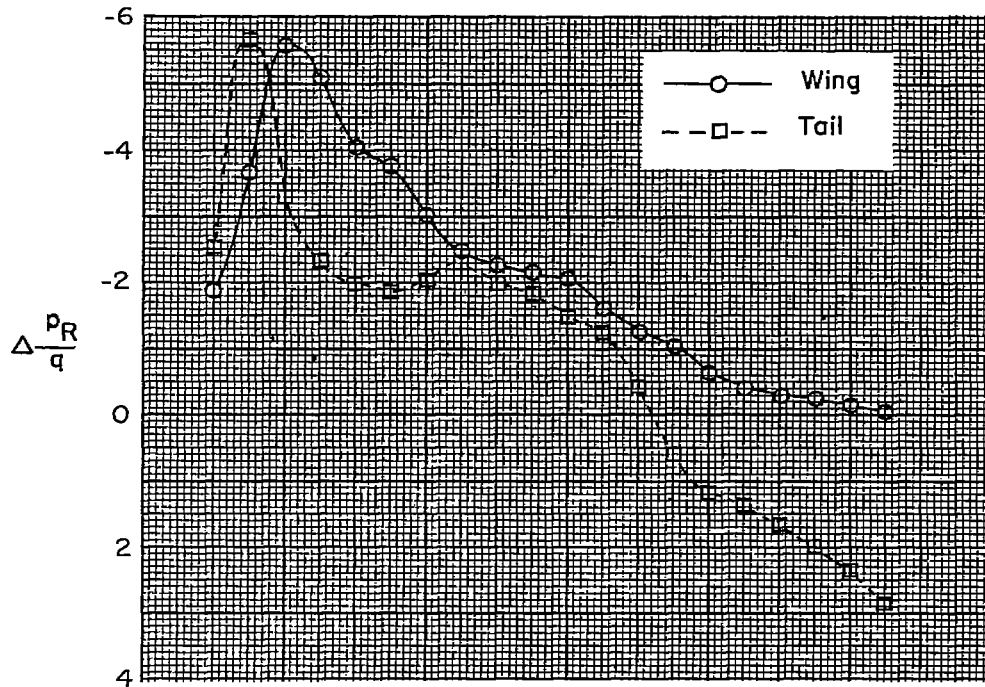
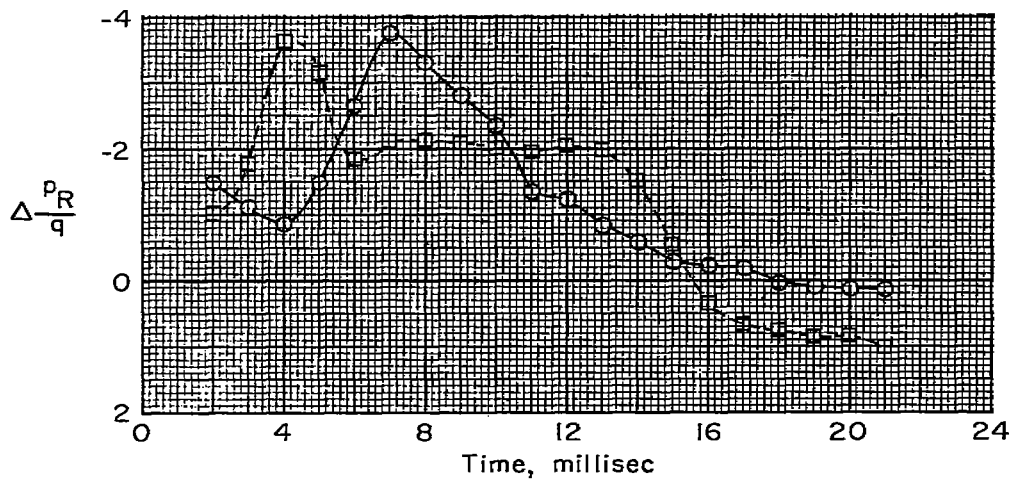


Figure 9.- Concluded.

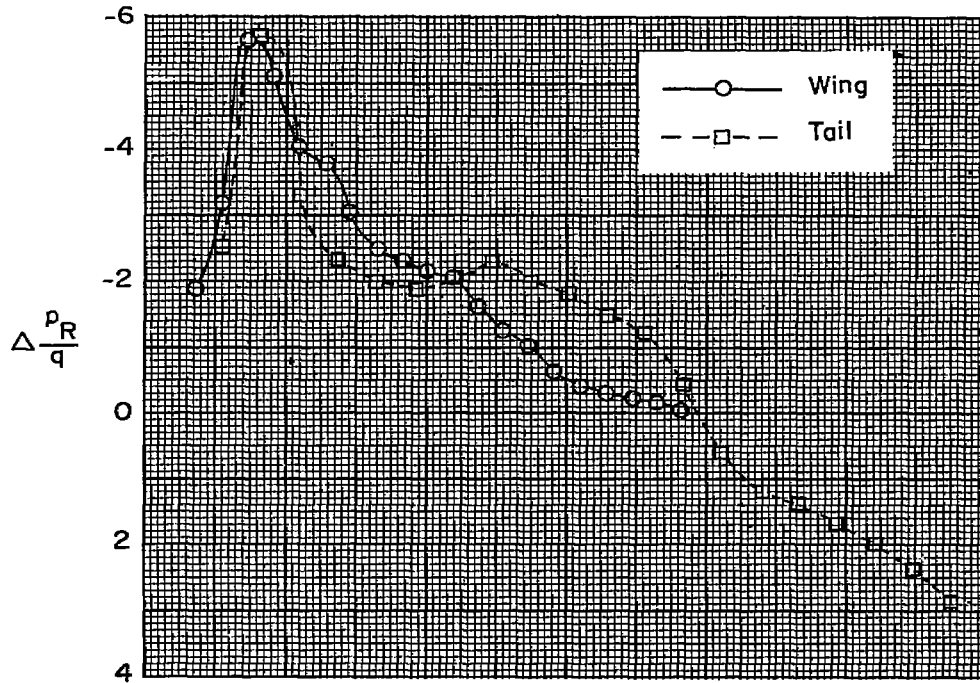


(a) Wing station, 0.19 chord; tail station, 0.20 chord.

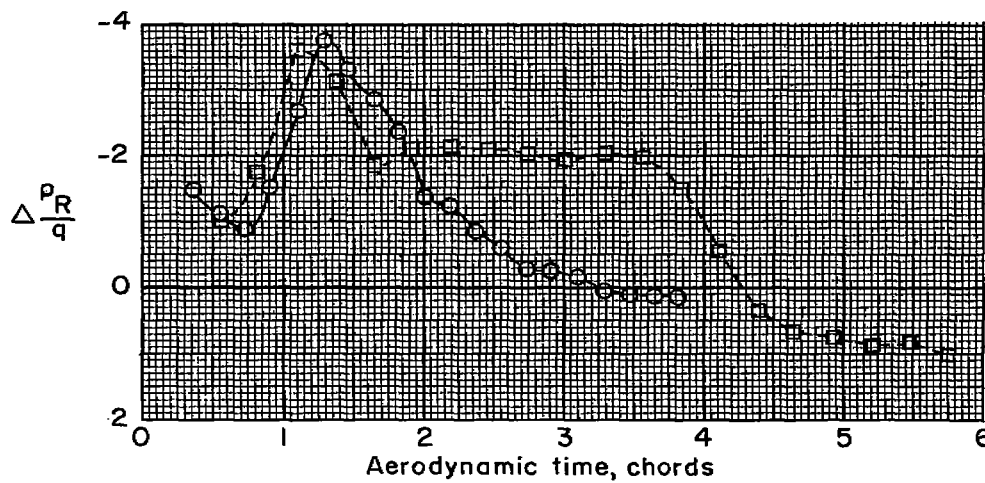


(b) Wing station, 0.37 chord; tail station, 0.40 chord.

Figure 10.- Comparison of average histories of load coefficients on wing and tail, absolute time.



(a) Wing station, 0.19 chord; tail station, 0.20 chord.



(b) Wing station, 0.37 chord; tail station, 0.40 chord.

Figure 11.- Comparison of average histories of load coefficients on wing and tail, aerodynamic time.

NASA Technical Library



3 1176 01437 7361

